Applied Physics B (2024) 130:77
https://doi.org/10.1007/s00340-024-08213-0

Applied Physics B
Lasers and Optics

RESEARCH

Snr-based beaconless multi-scan link acquisition model with vibration for LEO-to-ground laser communication

Sen Yang[1] · **Xiaofeng Li**[1]

Received: 26 January 2024 / Accepted: 23 March 2024 / Published online: 17 April 2024
© The Author(s), under exclusive licence to Springer-Verlag GmbH Germany, part of Springer Nature 2024

Abstract

We propose a link acquisition time model deeply involving the process from the transmitted power to received signal-to-noise ratio (SNR) for LEO-to-ground laser communication for the first time. Compared with the conventional acquisition models founded on geometry analysis with divergence angle threshold, utilizing SNR as the decision criterion is more appropriate for practical engineering requirements. Specially, under the combined effects of platform vibration and turbulence, we decouple the parameters of beam divergence angle, spiral pitch, and coverage factor at a fixed transmitted power for a given average received SNR threshold. Then the single-scan acquisition probability is obtained by integrating the field of uncertainty (FOU), probability distribution of coverage factor, and receiver field angle. Consequently, the closed-form analytical expression of acquisition time expectation adopting multi-scan, which ensures acquisition success, with essential reset time between single-scan is derived. The optimizations concerning the beam divergence angle, spiral pitch, and FOU are presented. Moreover, the influence of platform vibration is investigated. All the analytical derivations are confirmed by Monte Carlo simulations. Notably, we provide a theoretical method for designing the minimum divergence angle modulated by the laser, which not only improves the acquisition performance within a certain vibration range, but also achieves a good trade-off with the system complexity.

1 Introduction

The demand for larger bandwidth in modern satellite communication to handle vast amounts of data has rendered traditional radio frequency link with its low bandwidth and slow modulation rate impractical [1]. Free-space optics communication (FSOC), which offers several benefits such as a high bandwidth, use of a license-free spectrum, low power, and small form factor requirements, proves to be an excellent solution [2]. Over the past few decades, numerous missions have yielded valuable achievements and catalyzed technological advancements. Such as low-Earth orbit (LEO) to ground laser communication experiment of the STRV-2 module in 2000 [3], a repeatable 5.625 Gbps bidirectional laser communication at 1064 nm between the NFIRE satellite and an optical ground station [4], and a high-performance laser communication terminal developed by TESAT that fulfills the need of a power efficient system with a homodyne detection scheme and a BPSK modulation format [5].

The acquisition, pointing, and tracking (APT) system plays a crucial role in establishing a stable FSOC link between two terminals [6]. Some FSOC systems [7–9] employ the beacon strategy, which is commonly composed of two steps. First, the coarse APT emitting a beacon light with a large divergence angle and sufficient peak power is carried out to achieve a rough line-of-sight (LoS) alignment between the transmitter and receiver. Next, the transmitter employs a separate beam with a narrow divergence angle to enhance the alignment for fine APT [10]. The disadvantage of this beacon-based strategy is that it requires additional beacon laser, resulting in the large scale of FSOC system. Beaconless FSOC system has been proposed to simplify terminal structure and reduce power while maintaining performance compared to classical beacon-based strategy, where a narrow single beam is adopted both for APT and data transmission [11]. Subsequently, successful beaconless satellite-to-ground communication links were established

✉ Xiaofeng Li
lxf3203433@uestc.edu.cn

Sen Yang
yang_jansen@163.com

[1] School of Astronautics and Aeronautics, University of Electronic Science and Technology of China, Xiyuan Avenue, Chengdu 611731, Sichuan, China

using a compatible ground terminal [5], and operational considerations for the beaconless spatial acquisition were presented in [12]. However, the acquisition process poses significant challenges due to the narrow beam divergence angles and random vibration disturbances [10]. To address these challenges, analytic expressions and optimizations for multi-scan average acquisition time were presented in [13], taking into account factors such as the initial pointing error, beam divergence angle, and field of uncertainty (FOU). In addition, an approximate mathematical model was established in [14] to describe the influence of Gaussian random vibration on the acquisition probability. Furthermore, Ref. [15] derived an approximate analytical expression for the scan loss probability, considering the scanning parameters and platform vibrations, whose influence on acquisition time was analyzed under both single-scan and multi-scan patterns.

The mathematical models mentioned above assume that a successful acquisition requires the receiver to be within the beam divergence angle. They mainly focused on the first phase of the acquisition process, specifically on the scanning with which the beam enters the receiver antenna, lacking in-depth study on whether the optical signal incident on the photodetector can be effectively responded. In the APT system, photodetectors, such as four-quadrant detector of position sensors and charge-coupled device of image sensors, are utilized to correct the deviation of output spot [16, 17]. However, the sensor still has output even without beam incidence, which is caused by noise such as dark current [18]. If the response threshold is set too low, the noise will be misjudged as an optical signal, resulting in a false alarm. Conversely, If the threshold is set too high, the signal will be misjudged as noise, resulting in a missed detection. However, the absolute thresholds are different for types of sensors involving materials and other factors. Hence, signal-to-noise ratio (SNR) as a relative value becomes an appropriate indicator for criterion. Moreover, the optical intensity is also affected by the atmospheric turbulence in the satellite-to-ground laser communication [19], where SNR is further reduced. Therefore, the derivations only based on geometric analysis are not rigorous.

Ref. [20] investigated the acquisition performance with the determined power incident on the photodetector. It is a significant exploration, but the key parameter of transmitted power was not studied in depth in the model, which has the most direct and complete end-to-end relationship with the received SNR, as well as directly affects the complexity of the terminal structure. For LEO-to-ground [21] FSOC with a narrow acquisition window, the scanning needs to maintain the maximum transmitted power to achieve fast acquisition. However, there is no theoretical derivation and optimization of acquisition time model involving the entire process from the transmitted power to received SNR to the best of our knowledge. Spurred by the gap, the coverage factor, representing the ratio of the range of a beam to the spiral pitch wherein the received SNR over the threshold at a certain transmitted power, is first defined in Sect. 2. Then the power model is developed as a function of the beam divergence angle, the spiral pitch, and the coverage factor. Subsequently, we derive the probability distribution of the coverage factor, further combined with FOU and receiver field angle, we calculate the single-scan acquisition probability. In Sect. 3, given the essential reset time between single-scan, we establish a novel multi-scan acquisition time model. By utilizing the decoupled relationship between the beam divergence angle and the spiral pitch, the optimizations concerning the acquisition parameters, also including FOU, are presented. Moreover, the influence of platform vibration is investigated. Finally, Monte Carlo (MC) simulations are performed in Sect. 4 to verify the above theoretical derivations and optimization conclusions.

2 Single-scan mathematical model

During the establishment of a space laser link with beaconless APT, the signal beam divergence angle is markedly small, usually measured in microradians. While the discrepancy arising between the transmitter initial pointing and the LoS typically ranges in the magnitude of milliradians and exhibits a random distribution due to the accuracy errors from the satellite attitude, orbit prediction, and terminal control, resulting in the uncertainty of beam pointing. Consequently, the Archimedes spiral technique [22] is commonly adopted for scanning the FOU. While the receiver keeps staring at the transmitter. Once the receiver detects a laser signal that satisfies the specified SNR requirements, it calculates the spot deviation using the quantized response from the photodetector. The receiver then drives the high-precision servo mechanism to achieve a fine tuning on the pointing [23], and responds with an optical signal to stimulate the response of the photodetector at the transmitter, thereby completing the acquisition process. The acquisition diagram is depicted in Fig. 1.

2.1 Power model

Achieving global communication coverage typically requires the deployment of thousands of LEO satellites [25]. Some modulation and demodulation techniques within the direct detection system, such as pulse position modulation [26] and subcarrier index modulation [27], have achieved a good trade-off between communication rate and engineering cost, leading to their widespread adoption. The average SNR of 4QD within a direct detection system is defined as [24]:

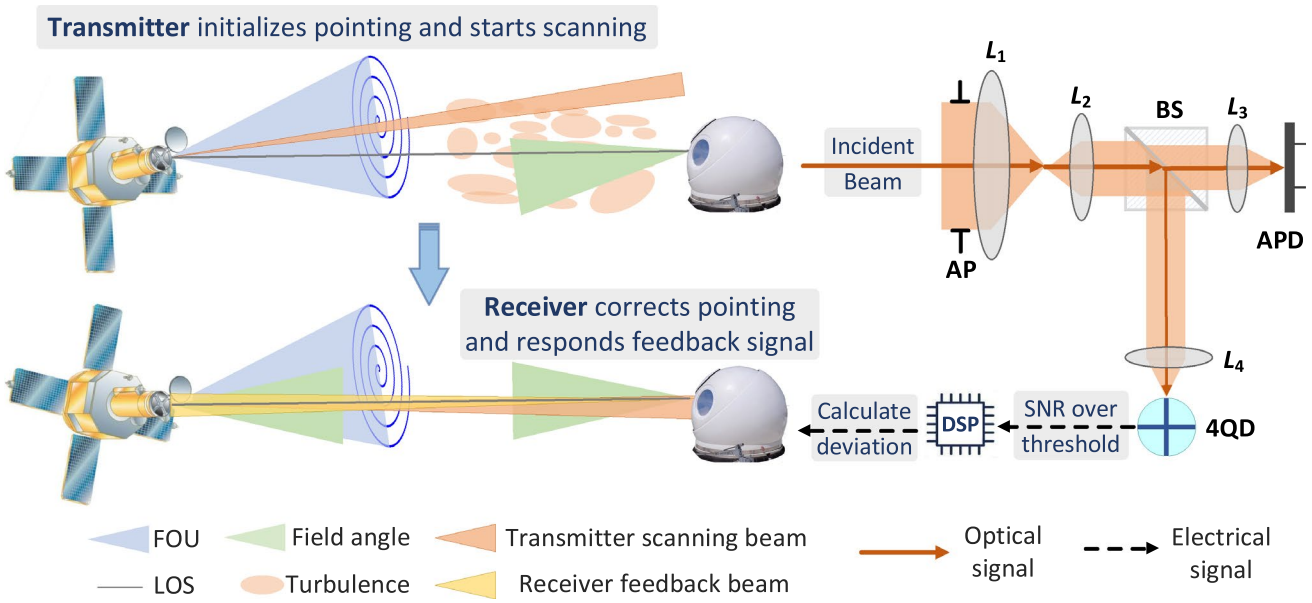

Fig. 1 The diagram of beaconless acquisition. The error arises between the satellite initial pointing (the center of the spiral) and the LoS. The LoS is covered by a blue conical shape, which allows the beam propagation towards the receiver antenna through scanning. Similarly, the green conical shape covers the LoS, enabling the received photons of the signal beam to fall on the photodetectors. The incident beam passes through an AP and is then expanded by the telescope system L_1-L_2. It subsequently passes through a BS and most of it is focused on an APD through L_3 for communication. The remaining small portion of the beam is detected by a 4QD through L_4 for spot deviation measurement. L_1, L_2, L_3, L_4, lens; AP, aperture; BS, beam splitter; APD, avalanche photo diode; 4QD, four-quadrant detector

$$\bar{Q} = \langle i_s^2 \rangle / \langle i_n^2 \rangle \tag{1}$$

where i_s is signal current, i_n is noise current, which is additive Gaussian white noise with zero mean and $\sigma_n^2 = N_0$ variance. There is $i_s = P_r R_r = P_t h_t h_c R_r$ in the direct detection system, P_t and P_r are the transmitter and receiver powers, respectively, h_t represents the transmission gain with vibration, h_c represents the turbulence attenuation, the two are independent [28], and R_r is photoelectric response efficiency. Therefore, Eq. (1) is specifically expressed as:

$$\bar{Q} = E[h_t^2] E[h_c^2] P_t^2 R_r^2 / N_0 \tag{2}$$

The scanning details are depicted in Fig. 2a. The optical signal is a Gaussian beam, whose divergence angle corresponding to $1/e^2$ intensity radius is ω. The distance between adjacent spiral arms is d, denoted as spiral pitch. The receiver may fall anywhere between adjacent spiral arms. The ideal scenario is on the spiral while the least favorable place would be on the midpoint of the adjacent spiral arms. To accommodate for this variability, $0 \le \tau \le 1/2$ is extracted as the coverage factor, representing the ratio of maximum acquisition deflection angle to spiral pitch that meets specified SNR level at the receiver for a certain transmitted power. In other words, the transmitted power can cover the circular range of radius τd, wherein the average SNR is greater than the threshold $\bar{Q}$.

Considering that the far-field propagation distance is R, the transmitter and receiver loss are s_t and s_r, respectively, the diameter of the receiving aperture is D_r, the proportion of split beam for acquisition is s_s, and the angle deviation between the transmitter pointing and LoS is φ. It should be noted that the distance between the satellite and the ground exceeds 1000 kms, so the radius of beam that reaches the receiving plane with a divergence angle of 10 micro radians is beyond 10 ms. On the other hand, the receiver aperture size is typically the order of decimeters. Based on these considerations, it can be assumed that the beam incident on the receiver aperture is uniform. Then the h_t is given by [29]:

$$h_t(\varphi) = \frac{2 s_t s_r s_s}{\pi R^2} \frac{1}{\omega^2} \exp\left(-\frac{2\varphi^2}{\omega^2}\right) \cdot \pi \left(\frac{D_r}{2}\right)^2 \tag{3}$$

where φ is a random variable influenced by platform vibration. The expectation of φ is τd, Generally, the variance of φ is isotropic, i.e., $\sigma_x = \sigma_y = \sigma \neq 0$, and the probability density function (PDF) of φ is the Rice distribution [14, 30]:

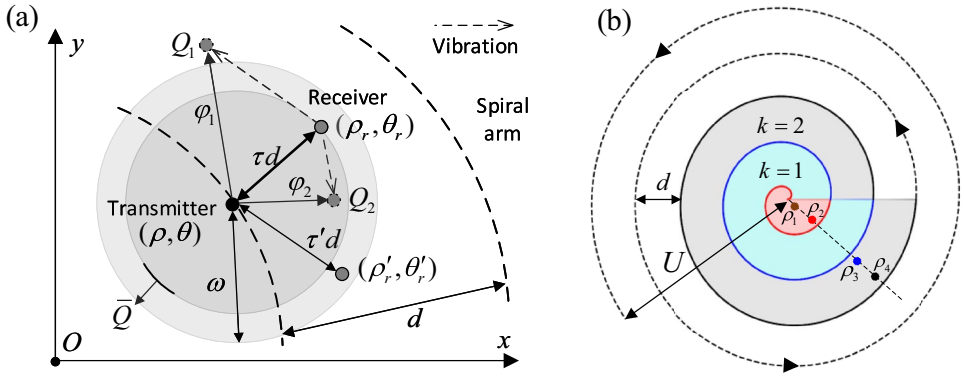

Fig. 2 Scanning diagram. **a** Details for scanning. d is spiral pitch, and ω is beam divergence angle. τd is the minimum distance between the receiver (ρ_r, θ_r) and the spirals. The platform vibration from transmitter is equivalent to the deviation on the receiver, so that $\varphi_n (n = 1, 2, \ldots)$ are random variables representing the angle deviation between the transmitter pointing and LoS. At a certain transmitted power, the corresponding instantaneous SNR are Q_n, and the received average SNR is equal to the threshold $\bar{Q}$, which is the lowest value in a circular region with transmitter (ρ, θ) as the center and τd as the radius. For the target (ρ_r', θ_r') with an angle deviation from the transmitter satisfying $\tau d < \tau' d < \omega$, its average SNR is less than the threshold although it is within the beam divergence angle, and the target will not feedback the optical signal, resulting in the acquisition failure. **b** Archimedean spiral scanning. U is field of uncertainty. The potential locations ρ_1 and ρ_2 of the receiver are within the central ring filled with red, they are acquired at the origin and on the red spiral, respectively. The blue section represents the $k = 1$ ring. Whereas ρ_3 and ρ_4 are located within the gray-filled $k = 2$ ring, they are acquired on the blue and the black spirals, respectively

$$f_\varphi(\varphi) = \frac{\varphi}{\sigma^2} \exp\left(-\frac{\varphi^2 + \tau^2 d^2}{2\sigma^2}\right) I_0\left(\frac{\varphi \tau d}{\sigma^2}\right) \tag{4}$$

where $I_0(\cdot)$ is the zero-order modified Bessel function of the first kind. Then we calculate $E\left[h_t^2\right]$:

$$\begin{aligned} E\left[h_t^2\right] &= \left(\frac{s_t s_r s_s D_r^2}{2R^2\omega^2}\right)^2 E_\varphi\left[\exp\left(-\frac{4\varphi^2}{\omega^2}\right)\right] \\ &= \left(\frac{s_t s_r s_s D_r^2}{2R^2}\right)^2 \frac{1}{\omega^2\left(\omega^2 + 8\sigma^2\right)} \\ &\quad \exp\left(-\frac{4\tau^2 d^2}{\omega^2 + 8\sigma^2}\right) \end{aligned} \tag{5}$$

The atmospheric turbulence is modeled by the Gamma-Gamma distribution in order to cover a wide range of turbulence conditions [31]. Subsequently, the $E\left[h_c^2\right]$ is obtained as [32]:

$$E\left[h_c^2\right] = \frac{(\alpha + 1)(\beta + 1)\gamma^2}{\alpha\beta} \tag{6}$$

where γ is the scale parameter. α and β are large-scale and small-scale effective numbers, respectively, which can directly be linked to the physical parameter Rytov variance [33]. Atmospheric turbulence can induce fluctuations in the received intensity, which are commonly characterized by the scintillation index (SI). In the Gamma-Gamma model, the SI σ_l^2 is defined as follows [24]:

$$\sigma_l^2 = \frac{\left\langle h_c^2 \right\rangle}{\left\langle h_c \right\rangle^2} - 1 = \frac{1}{\alpha} + \frac{1}{\beta} + \frac{1}{\alpha\beta} \tag{7}$$

Combining Eqs. (2), (5), and (6) yields the specific expression of P_t:

$$\begin{aligned} P_t = &\frac{2R^2}{s_t s_r s_s \gamma D_r^2 R_r} \sqrt{\frac{\bar{Q} N_0 \alpha\beta}{(\alpha + 1)(\beta + 1)}} \\ &\omega\sqrt{\omega^2 + 8\sigma^2} \exp\left(\frac{2\tau^2 d^2}{\omega^2 + 8\sigma^2}\right) \end{aligned} \tag{8}$$

For the LEO-to-ground FSOC with a limited narrow window, the transmitter needs to scan at the maximum power to achieve acquisition in the shortest time, namely P_t is a constant. Then we solve the relationship between τ, d, and ω:

$$\tau d = g_{B,\sigma}(\omega) = \sqrt{\frac{\omega^2 + 8\sigma^2}{2} \ln\left(\frac{B}{\omega\sqrt{\omega^2 + 8\sigma^2}}\right)} \tag{9}$$

where $B = \frac{P_t s_t s_r s_s \gamma D_r^2 R_r}{2R^2} \sqrt{\frac{(\alpha+1)(\beta+1)}{\bar{Q} N_0 \alpha\beta}}$. Meanwhile, we obtain the constraint on ω from Eq. (9):

$$\ln\left(\frac{B}{\omega\sqrt{\omega^2 + 8\sigma^2}}\right) > 0 \rightarrow \omega < \sqrt{\sqrt{B^2 + 16\sigma^4} - 4\sigma^2} \tag{10}$$

2.2 Acquisition time model

The polar coordinate (ρ, θ) in Fig. 2a represents the scanning trajectory on the spiral arm, where θ increments by 2π with each spiral turn. The Archimedean spiral is parameterized as $\rho = d\theta/(2\pi)$ [22].

The position of the receiver, also known as the initial pointing error, follows a Gaussian distribution with zero mean, and the variances (κ_x, κ_y) are equal in both the horizontal and vertical directions, i.e. $\kappa_x = \kappa_y = \kappa$. The corresponding polar coordinate is (ρ_r, θ_r), where the polar angle θ_r adheres to a uniform distribution $U(0, 2\pi)$, and the radial ρ_r obeys the Rayleigh distribution:

$$f_{\rho_r}(\rho_r) = \frac{\rho_r}{\kappa^2} \exp\left(-\frac{\rho_r^2}{2\kappa^2}\right) \tag{11}$$

In addition, we introduce the definition of a ring, which is the area enclosed by spirals with an increment of θ by 2π, as depicted in Fig. 2b. Notably, the ring having $\theta \in [0, 2\pi)$ is considered special because its inner degenerates to the origin and the distance between the outer spiral and the inner spiral (origin) is $\frac{d}{2\pi}\theta < d$, thus named the central ring. The others in the range of $\theta \in [2k\pi, 2k\pi + 2\pi)$, $k = 1, 2, \ldots$, are specified as k rings, where the distance between the outer and the inner spirals is d. For each k ring, the inner spiral refers to the outer spiral of the previous ring, and correspondingly, the outer spiral denotes the inner spiral of the next ring. Consequently, by combining Eq. (11) and $\theta_r \sim U(0, 2\pi)$, we obtain the PDF with respect to the coverage factor τ as:

$$\begin{aligned} f_\tau(\tau) = \frac{1}{2\pi} \int \Bigg[& f_{\rho_r}(\rho_1) \left|\frac{d\rho_1}{d\tau}\right|_{\rho_1=\tau d} \\ & + f_{\rho_r}(\rho_2) \left|\frac{d\rho_2}{d\tau}\right|_{\rho_2=(\frac{\theta_r}{2\pi}-\tau)d} \Bigg] d\theta_r \\ & + \frac{1}{2\pi} \sum_{k=1}^{\infty} \int \Bigg[f_{\rho_r}(\rho_3) \left|\frac{d\rho_3}{d\tau}\right|_{\rho_3=(\frac{\theta_r}{2\pi}+k-1+\tau)d} \\ & + f_{\rho_r}(\rho_4) \left|\frac{d\rho_4}{d\tau}\right|_{\rho_4=(\frac{\theta_r}{2\pi}+k-\tau)d} \Bigg] d\theta_r \end{aligned} \tag{12}$$

where the acquisition point of ρ_1 is the central ring origin, the position for ρ_2 is on the outer spiral of the central ring, whereas ρ_3 and ρ_4 are acquired on the inner and the outer spirals of the k ring, as illustrated in Fig. 2b For k rings, the distance from the receiver to the spiral where the acquisition point is located is τd, while the distance to the other spiral is $(1-\tau)d$. Since $0 \le \tau \le \frac{1}{2}$, it always holds true that $\tau d \le (1-\tau)d$ for any $[0, 2\pi]$. As for the central ring, the distance from the receiver to the acquisition spiral is also τd, but the distance to the other spiral is $\frac{d}{2\pi}\theta_r - \tau d$, which means that θ_r needs to satisfy the additional constraint $\tau d \le \frac{d}{2\pi}\theta_r - \tau d$ for a given τ, i.e., $4\pi\tau \le \theta_r \le 2\pi$. Then Eq. (12) is integrated as:

$$\begin{aligned} f_\tau(\tau) = & \left(\frac{(1-2\tau)\tau d^2}{\kappa^2} + 1\right) \exp\left(-\frac{\tau^2 d^2}{2\kappa^2}\right) \\ & - \exp\left(-\frac{(\tau-1)^2 d^2}{2\kappa^2}\right) \\ & + \sum_{k=1}^{\infty} \Bigg[\exp\left(-\frac{(k-1+\tau)^2 d^2}{2\kappa^2}\right) \\ & - \exp\left(-\frac{(k+\tau)^2 d^2}{2\kappa^2}\right) \\ & - \exp\left(-\frac{(k+1-\tau)^2 d^2}{2\kappa^2}\right) + \exp\left(-\frac{(k-\tau)^2 d^2}{2\kappa^2}\right) \Bigg] \\ = & \left[\frac{(1-2\tau)\tau d^2}{\kappa^2} + 2\right] \exp\left(-\frac{\tau^2 d^2}{2\kappa^2}\right) \end{aligned} \tag{13}$$

When the closest distance between the spirals and the receiver is less than τd, the received average SNR is greater than the threshold, namely the transmitted power can cover the receiver given the SNR threshold, yielding a successful detection. Hence, the probability P_{SNR} that the received average SNR over the threshold is the CDF of coverage factor:

$$\begin{aligned} P_{SNR} = & P(\mathcal{T} \le \tau) = \int_0^{\tau} f_\tau(\mathcal{T}) d\mathcal{T} \\ = & 1 + (2\tau - 1) \exp\left(-\frac{\tau^2 d^2}{2\kappa^2}\right) \end{aligned} \tag{14}$$

Actually, κ is milliradian magnitude, and d is microradian magnitude, i.e., $\kappa \gg d$. Hence, τ approximately obeys uniform distribution $U(0, 1/2)$, and Eq. (14) is reduced as $P_{SNR} \approx 2\tau$.

Moreover, the signal is likely to be detected when LoS is within the field angle range of the receiver. The corresponding field detection probability P_V is obtained as:

$$P_V = \int_0^V f_{\rho_r}(\rho_r) d\rho_r = 1 - \exp\left(-\frac{V^2}{2\kappa^2}\right) \tag{15}$$

where V represents the half-width of the field angle of the photoelectric sensor at the receiver. Hence $0 < P_V < 1$ is independent of the scanning parameters of the transmitter and can be regarded as a constant. Then we define the feedback probability of the receiver as $P_R = P_V \cdot P_{SNR} = 2P_V\tau$.

Furthermore, the acquisition is likely to be successful when the receiver (ρ_r, θ_r) within the range of FOU, defined as U and shown in Fig. 2b. The corresponding probability P_U is expressed as [13]:

$$P_U = \int_0^U f_{\rho_r}(\rho_r)d\rho_r = 1 - \exp\left(-\frac{U^2}{2\kappa^2}\right) \tag{16}$$

Consequently, the probability of single-scan acquisition is:

$$P_S = P_U \cdot P_R \tag{17}$$

As shown in Fig. 2b, the scanning usually adopts the Archimedean spiral to achieve an efficient search from high probability to low probability regions. We define $a = d/(2\pi)$, and the length of the Archimedean spiral is given by [22]:

$$L = \frac{1}{2}\left[\rho_r\sqrt{1+\left(\frac{\rho_r}{a}\right)^2} + a\ln\left(\frac{\rho_r}{a} + \sqrt{1+\left(\frac{\rho_r}{a}\right)^2}\right)\right] \tag{18}$$

In general $\rho_r \gg a$ so that Eq. (18) is approximated by $L \approx \rho_r^2/(2a)$. Then the single-scan acquisition time is calculated with constant scanning speed v as $t_S = \pi\rho_r^2/(vd)$. Combining with Eq. (11) yields the PDF of t_S:

$$f_{t_S}(t_S) = \frac{vd}{2\pi\kappa^2}\exp\left(-\frac{vd}{2\pi\kappa^2}t_S\right) \tag{19}$$

Subsequently, the time expectation T_S for the single-scan acquisition is:

$$\begin{aligned} T_S &= \int_0^{T_U} t_S \cdot f_{t_S}(t_S)dt_S \\ &= \frac{2\pi\kappa^2}{vd}\left[1 - \exp\left(-\frac{U^2}{2\kappa^2}\right)\left(1+\frac{U^2}{2\kappa^2}\right)\right] \end{aligned} \tag{20}$$

where $T_U = \pi U^2/(vd)$ is the time for scanning the complete FOU.

3 Multi-scan mathematical model

Acquisition success cannot be guaranteed with only once single-scan due to $P_S < 1$. Therefore, the multi-scan, which is a series of repetitive scans over the same FOU, is often employed instead. In particular, when a single-scan proves failure, it is necessary to reinitialize the transmitter pointing based on ephemeris table and repeat the single-scan until a successful acquisition is achieved [13]. In this process, reset time T_a for the APT to reinitialize the pointing to prepare for the next single-scan is strongly essential but ignored by previous analytical models. Therefore, when the acquisition is achieved in $n+1$ single-scan, the total scanning time t_M is:

$$t_M = n(T_U + T_a) + t_S \tag{21}$$

The PDF of t_M is:

$$f_{t_M}(t_M) = (1-P_S)^n P_R f_{t_S}(t_S) \tag{22}$$

Then we calculate the CDF of t_M as:

$$\begin{aligned} P(T \le t_M) &= P(T \le n(T_U + T_a)) \\ &\quad + P(n(T_U + T_a) < T \le t_M) \\ &= \sum_{k=0}^{n-1}(1-P_S)^k P_R \int_0^{T_U} f_{t_S}(T)dT \\ &\quad + (1-P_S)^n P_R \int_0^{t_S} f_{t_S}(T)dT \\ &= 1 - (1-P_S)^n\left\{1 - P_R\left[1 - \exp\left(-\frac{vd}{2\pi\kappa^2}t_S\right)\right]\right\} \end{aligned} \tag{23}$$

There is $n \to \infty$ and $t_S \to T_U$ for $t_M \to \infty$. Then the acquisition probability of Eq. (23) becomes:

$$\lim_{t_M\to\infty} P(T \le t_M) = \lim_{n\to\infty}\left[1 - (1-P_S)^{n+1}\right] = 1 \tag{24}$$

which proves that the multi-scan can ensure acquisition success. The acquisition time expectation T_M with multi-scan is calculated as:

$$\begin{aligned} T_M &= \int_0^\infty t_M \cdot f_{t_M}(t_M)dt_M \\ &= \sum_{n=0}^\infty (1-P_S)^n P_R \int_0^{T_U}\left[n(T_U+T_a) + t_S\right]\cdot f_{t_S}(t_S)dt_S \\ &= \sum_{n=0}^\infty (1-P_S)^n P_S\left[\frac{T_S}{P_U} + n(T_U+T_a)\right] \\ &= \frac{T_S}{P_U} + \left(\frac{1}{P_S} - 1\right)(T_U + T_a) \\ &= \frac{2\pi\kappa^2}{vd}\left[\frac{e^\eta\eta(1-P_R)}{(e^\eta-1)P_R} + 1\right] \\ &\quad + \frac{T_a\left[e^\eta(1-P_R) + P_R\right]}{(e^\eta-1)P_R} \end{aligned} \tag{25}$$

where $\eta = U^2/(2\kappa^2) > 0$. Given that ω, d, and τ are coupled according to Eq. (9), where any two known terms can solve the remaining one theoretically. However, ω cannot be uniquely determined by τ and d. Since d only appears once in Eq. (25), we replace d to facilitate subsequent optimization analysis for the goal of minimizing T_M.

3.1 Spiral pitch optimization

When $g_{B,\sigma}(\omega)/d > 1/2$, there is $\tau \equiv 1/2$ with $P_R = P_V$ in Eq. (25), where T_M is not related to τ and it decreases with d. The minimum is taken at $d = 2g_{B,\sigma}(\omega)$.

While $g_{B,\sigma}(\omega)/d \le 1/2$, the derivative of T_M with respect to τ by replacing $d = g_{B,\sigma}(\omega)/\tau$ in Eq. (25) is:

$$\frac{\partial T_M}{\partial \tau} = \frac{2\pi\kappa^2(e^\eta - e^\eta\eta - 1)}{v(e^\eta-1)\cdot g_{B,\sigma}(\omega)} - \frac{2e^\eta P_V T_a}{(e^\eta-1)P_R^2} \tag{26}$$

where T_M decreases monotonically with τ due to $(e^{\eta} - e^{\eta}\eta - 1)$ constantly less than zero. The minimum T_M is taken at $\tau_{opt} = 1/2$. Consequently, the optimum spiral pitch d_{opt} is:

$$d_{opt} = 2g_{B,\sigma}(\omega) = \sqrt{2\left(\omega^2 + 8\sigma^2\right)\ln\left(\frac{B}{\omega\sqrt{\omega^2 + 8\sigma^2}}\right)} \tag{27}$$

3.2 Beam divergence angle optimization

By the same token, T_M is independent of ω when $g_{B,\sigma}(\omega)/d > 1/2$, thus T_M does not change with ω in this case.

While $g_{B,\sigma}(\omega)/d \le 1/2$, the derivative of T_M with respect to ω by replacing $d = g_{B,\sigma}(\omega)/\tau$ is:

$$\begin{aligned}\frac{\partial T_M}{\partial \omega} &= \frac{\partial T_M}{\partial g_{B,\sigma}}\frac{\partial g_{B,\sigma}}{\partial \omega} \\ &= -\frac{\pi\kappa^2\left[e^{\eta}\eta\left(1 - P_R\right) + P_R(e^{\eta} - 1)\right]}{v(e^{\eta} - 1)P_V \cdot g_{B,\sigma}^2(\omega)} \\ &\quad \times \frac{\omega^2 \ln\left(\frac{B}{\omega\sqrt{\omega^2+8\sigma^2}}\right) - \omega^2 - 4\sigma^2}{2\omega \cdot g_{B,\sigma}(\omega)}\end{aligned} \tag{28}$$

Let $\partial T_M/\partial\omega = 0$, i.e., $\partial g_{B,\sigma}/\partial\omega = 0$, and obtain:

$$B = B_\sigma(\omega) = \omega\sqrt{\omega^2 + 8\sigma^2}\exp\left(1 + \frac{4\sigma^2}{\omega^2}\right) \tag{29}$$

The derivative of $B_\sigma(\omega)$ concerning ω is:

$$\frac{\partial B_\sigma}{\partial \omega} = \frac{2\left(\omega^4 - 32\sigma^4\right)}{\omega^2\sqrt{\omega^2 + 8\sigma^2}}\exp\left(1 + \frac{4\sigma^2}{\omega^2}\right) \tag{30}$$

where B_σ decreases for $\omega < 2^{5/4}\sigma$ and increases for $\omega > 2^{5/4}\sigma$. The minimum B_σ is reached at $\omega = 2^{5/4}\sigma$, namely $B_\sigma^{\min} = B_\sigma\left(2^{5/4}\sigma\right)$.

Thereby, when $B \le B_\sigma^{\min}$, there is $\partial g_{B,\sigma}/\partial\omega < 0$ and $\partial T_M/\partial\omega > 0$, T_M increases monotonically with ω in this case, and the minimum value is taken at ω_{limit}, which is the minimum divergence angle that the laser device can modulate.

When $B > B_\sigma^{\min}$, T_M has two extreme points $B_\sigma\left(\omega_{top}\right) = B_\sigma\left(\omega_{btm}\right) = B$, where ω_{top} is the maximum point in $\left(0, 2^{5/4}\sigma\right]$, and ω_{btm} is the minimum in $\left(2^{5/4}\sigma, +\infty\right)$, both are within the range of Eq. (10). Obviously, there must be a point $\omega_{eq} \in \left(0, 2^{5/4}\sigma\right]$ that satisfies $T_M\left(\omega_{eq}\right) = T_M\left(\omega_{btm}\right)$. Consequently, the minimum T_M is obtained at ω_{btm} for $\omega_{eq} \le \omega_{limit} \le \omega_{btm}$ or at ω_{limit} for $\omega_{limit} < \omega_{eq}$ or $\omega_{limit} > \omega_{btm}$, but the analytical expression of ω_{eq} is unsolvable. Fortunately, we can take advantage of the known quantities B and ω_{limit} to determine the optimum beam divergence angle ω_{opt} by indirect derivation and comparison.

As deduced before, $B_\sigma\left(\omega_{limit}\right)$ monotonically increases when $\omega_{limit} \ge 2^{5/4}\sigma$. If $B_\sigma\left(\omega_{btm}\right) = B < B_\sigma\left(\omega_{limit}\right)$, there is $\omega_{btm} < \omega_{limit}$ and the minimum T_M is obtained at ω_{limit}, otherwise at ω_{btm}.

It can be found from Eq. (28) that the trends of T_M and $g_{B,\sigma}$ with ω are opposite. Thereby the minimum of $g_{B,\sigma}$ for $\omega \in \left(0, 2^{5/4}\sigma\right]$ is taken at ω_{top}, and the corresponding minimum is calculated by substituting $B = B_\sigma\left(\omega_{top}\right)$ into $g_{B,\sigma}\left(\omega_{top}\right)$ as:

$$\begin{aligned}g_{B,\sigma}\left(\omega|\omega \le 2^{5/4}\sigma\right) &\ge g_{B,\sigma}\left(\omega_{top}\right) \\ &= \sqrt{\frac{\left(\omega_{top}^2 + 8\sigma^2\right)\left(\omega_{top}^2 + 4\sigma^2\right)}{2\omega_{top}^2}} \ge \left(2 + \sqrt{2}\right)\sigma\end{aligned} \tag{31}$$

If ω_{eq} is known, ω_{btm} can be solved by $g_{B,\sigma}\left(\omega_{eq}\right) = g_{B,\sigma}\left(\omega_{btm}\right)$ as:

$$\omega_{btm} = W(A) = \sqrt{A^2 - 6\sigma^2 + \sqrt{A^4 - 12A^2 + 4\sigma^4}} > 2^{5/4}\sigma \tag{32}$$

where $A = g_{B,\sigma}\left(\omega_{eq}\right)$ with constraint $A \ge \left(2 + \sqrt{2}\right)\sigma$, which is exactly consistent with Eq. (31), thus ω_{btm} certainly exist and increases monotonically with A. Additionally, we obtain ω'_{btm} by substituting $A' = g_{B,\sigma}\left(\omega_{limit}\right)$ into Eq. (32) for $\omega_{limit} < 2^{5/4}\sigma$. If $B = B_\sigma\left(\omega_{btm}\right) < B_\sigma\left(\omega'_{btm}\right)$, there is $\omega_{btm} < \omega'_{btm}$, further $g_{B,\sigma}\left(\omega_{eq}\right) = A < A' = g_{B,\sigma}\left(\omega_{limit}\right)$, thus $T_M\left(\omega_{limit}\right) < T_M\left(\omega_{eq}\right) = T_M\left(\omega_{btm}\right)$, the minimum T_M is obtained at ω_{limit}. Otherwise at ω_{btm}. Consequently, the optimum beam divergence angle ω_{opt} is:

$$\omega_{opt} = \begin{cases} \omega_{limit}, & B < B_\sigma\left(W\left(g_{B,\sigma}(\omega_{limit})\right)\right) \text{ with } \omega_{limit} < 2^{5/4}\sigma \\ & B < B_\sigma\left(\omega_{limit}\right) \text{ with } \omega_{limit} \ge 2^{5/4}\sigma \\ \omega_{btm}, & \text{else} \end{cases} \text{ or} \tag{33}$$

When $\omega_{btm}^2 \gg 4\sigma^2$, Eq. (29) is approximated as:

$$\begin{aligned}\frac{B}{e} &= \omega\sqrt{\omega^2 + 8\sigma^2} \cdot \exp\left(\frac{4\sigma^2}{\omega^2}\right) \\ &\approx \omega\sqrt{\omega^2 + 8\sigma^2}\left(1 + \frac{4\sigma^2}{\omega^2}\right) \\ &= \left(\omega^2 + 4\sigma^2\right)\sqrt{1 + \frac{8\sigma^2}{\omega^2}} \\ &\approx \left(\omega^2 + 4\sigma^2\right)\left(1 + \frac{4\sigma^2}{\omega^2}\right) = \left(\omega + \frac{4\sigma^2}{\omega}\right)^2\end{aligned} \tag{34}$$

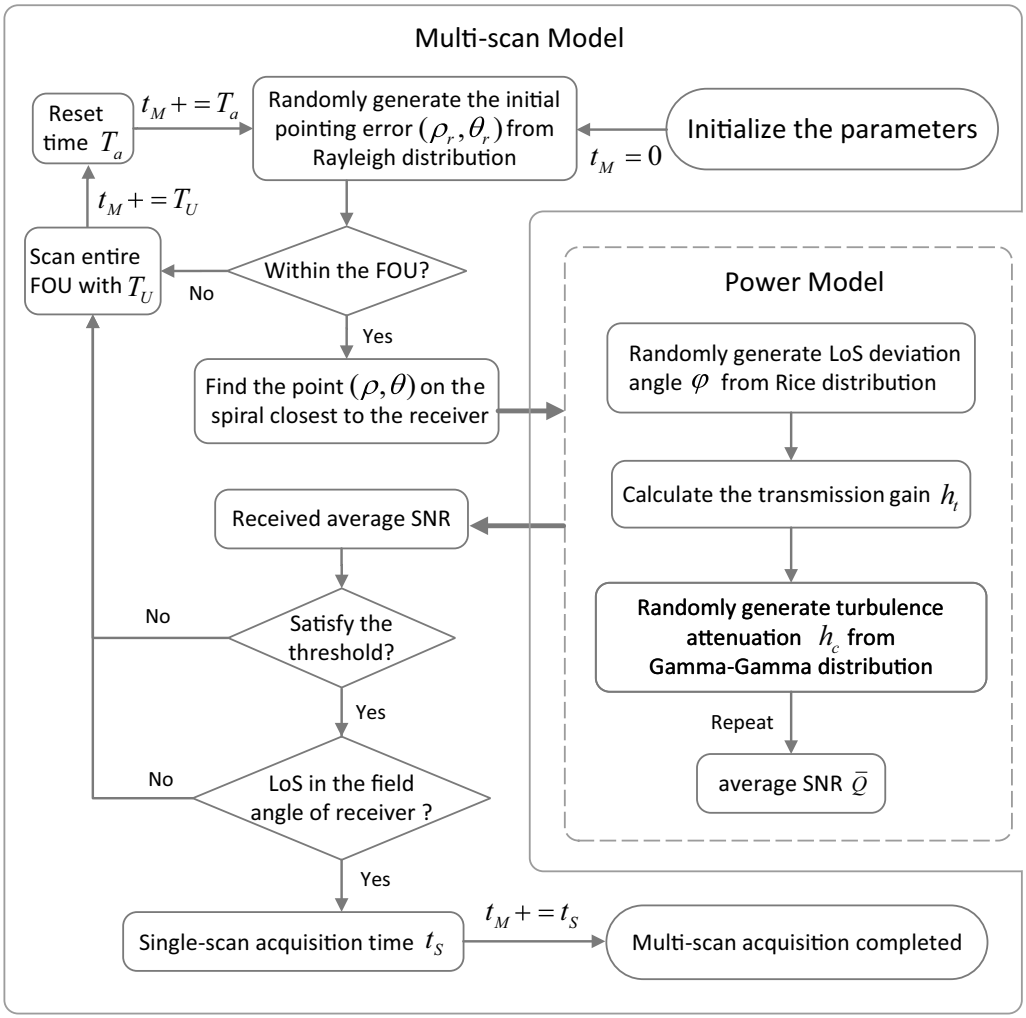

Fig. 3 Simulation process of Monto Carlo

Therefore, the approximate analytical ω_{btm} can be solved, whose the difference from the numerical solutions is within 0.1% in the case of $B \geq 2B_{\sigma}^{\min}$.

However, the value of ω_{btm} decreases as B get smaller than $2B_{\sigma}^{\min}$ so that the approximate error becomes larger. We adopt polynomials to fit the numerical solutions of Eq. (29), where the goodness of fit (GoF) is utilized as an index to evaluate the fitting accuracy. The variable is $x = B/B_{\sigma}^{\min}$ and fit in $[1, 2)$ with $GoF = 0.999$. The piecewise ω_{btm} is expressed as:

$$\omega_{btm} = \begin{cases} \left(1.5087x^3 - 7.9617x^2 + 15.913x - 6.8278\right)\sigma, & 1 \leq x < 2 \\ \dfrac{\sqrt{B} + \sqrt{B - 16e\sigma^2}}{2\sqrt{e}}, & 2 \leq x \end{cases} \tag{35}$$

3.3 FOU optimization

The derivative of T_M with respect to η is:

$$\frac{\partial T_M}{\partial \eta} = \frac{2\pi\kappa^2 e^{\eta}\left(1 - P_R\right)\left(e^{\eta} - \eta - 1 - \hat{T}_a\right)}{vd(e^{\eta} - 1)^2 P_R} \tag{36}$$

where $\hat{T}_a = \frac{vd \cdot T_a}{2\pi\kappa^2(1-P_R)}$, the minimum T_M is taken at $\partial T_M / \partial \eta = 0$, i.e., $e^{\eta} - \eta - 1 - \hat{T}_a = 0$. However, this equation has no analytical solution. When η is large, there is approximate $\eta \approx \ln(\hat{T}_a)$, which can be employed as the variable to perform polynomial fitting with numerical solutions and effectively reduce the order. In general, v and κ are of the same order of magnitude, which is three orders larger than d. T_a and $(1 - P_R)$ are the level of 10^1 and 10^{-2}, respectively. Therefore, $\hat{T}_a$ is about $10^{-1} \sim 10^0$ magnitude order. Without loss of generality, we perform piecewise

fitting in the interval $[0.01, 10]$ with $GoF = 0.999$. Consequently, the fitting polynomials for $x = \ln(\hat{T}_a)$ is:

$$\eta_{opt} = \begin{cases} 0.02824x^2 + 0.3137x + 0.9873, & 0.01 \le \hat{T}_a < 0.1 \\ 0.06114x^2 + 0.4549x + 1.1445, & 0.1 \le \hat{T}_a \le 1 \\ 0.07171x^2 + 0.4725x + 1.1441, & 1 < \hat{T}_a \le 10 \end{cases} \tag{37}$$

Then the optimum FOU is $U_{opt} = \kappa\sqrt{2\eta_{opt}}$.

3.4 Platform vibration influence

It can be found in Eq. (33) that the optimum beam divergence angle changes with the vibration standard deviation. Hence, the analysis of the vibration influence on the multi-scan acquisition time is significant. Through the principle of composite derivation, we get:

$$\begin{aligned} \frac{\partial T_M}{\partial \sigma} &= \frac{\partial T_M}{\partial g_{B,\sigma}}\left(\frac{\partial g_{B,\sigma}}{\partial \sigma} + \frac{\partial g_{B,\sigma}}{\partial \omega}\frac{\partial \omega}{\partial \sigma}\right) \\ &= -\frac{\pi\kappa^2\left[e^{\eta}\eta\left(1-P_R\right)+P_R(e^{\eta}-1)\right]}{v(e^{\eta}-1)P_V \cdot g_{B,\sigma}^2(\omega)} \\ &\quad \times \left[\frac{4\ln\left(\frac{B}{\omega\sqrt{\omega^2+8\sigma^2}}\right)-2}{g_{B,\sigma}(\omega)} + \frac{\partial g_{B,\sigma}}{\partial \omega}\frac{\partial \omega}{\partial \sigma}\right] \end{aligned} \tag{38}$$

When $\omega_{opt} = \omega_{limit}$, the divergence angle is constant thus $\partial\omega/\partial\sigma = 0$. T_M increases monotonically with σ for $\omega_{limit} > B^{1/2}e^{-1/4}$. While for $\omega_{limit} \le B^{1/2}e^{-1/4}$, the optimum is taken at $\partial T_M/\partial\sigma = 0$, i.e., $\sigma_{opt} = \sqrt{B^2 - e\omega^4}/\left(2\sqrt{2e}\omega\right)$. Therefore, the corresponding $\omega_{\sigma,limit}$ is solved with the known standard deviation σ of platform vibration as:

$$\omega_{\sigma,limit} = \sqrt{\sqrt{B^2/e + 16\sigma^4} - 4\sigma^2} \tag{39}$$

which is in the range of Eq. (10). We design ω_{limit} by referring to Eq. (39), whose rationality is reflected in that the change of vibration intensity leads to an increase in acquisition time.

When $\omega_{opt} = \omega_{btm}$, there is $\partial g_{B,\sigma}/\partial\omega = 0$ and $4\ln\left(\frac{B}{\omega\sqrt{\omega^2+8\sigma^2}}\right) - 2 = 2 + \frac{16\sigma^2}{\omega^2} > 0$ according to Eq. (28), further T_M decreases with σ.

4 Discussion of the results

The numerical results are presented as an illustration of the above derivations. The MC simulations with respect to the downlink acquisition are also performed to verify the obtained analytical expressions. The simulation process is illustrated in Fig. 3, and the corresponding parameters are listed in Table 1. Note that the time for LEO-to-ground link acquisition is relatively short, and during this period, the atmospheric environment remains relatively stable. Therefore, we assume that the turbulence channel parameters remain constant for each acquisition simulation.

Figure 4 depicts the variation of the multi-scan acquisition time with the spiral pitch under different turbulences, where $\omega = 20\mu rad$ and $U = 1.3mrad$. The simulation process is illustrated as the multi-scan model in Fig. 3. The theoretical acquisition time and the optimum spiral pitch can be calculated according to Eqs. (25) and (27), respectively. It should be noted that $g_{B,\sigma}(\omega)/d$ exceeds the upper limit of $\tau \in [0, 1/2]$ for $d < d_{opt}$, thus the corresponding coverage factor is identified as 1/2. In Ref. [14], the acquisition probability is related to the ratio of the beam divergence angle to the spiral pitch, and the greater the ratio, the greater the acquisition probability. When the pitch is less than $22\mu rad$, the acquisition probability is approximate to one, thus it is close to the simulation results. Due to the lack of consideration on transmitted power and turbulence in [14], the acquisition probability yields a large deviation for the pitch greater than $22\mu rad$, and the acquisition time is significantly different from the simulation results. While our theoretical results are in good agreement with the corresponding MC results, which demonstrate the multi-scan model. Moreover, the acquisition time increases with the spiral pitch when $d \ge d_{opt}$, which is because the decrease of the corresponding coverage factor results in the decrease of single-scan acquisition probability. While $d < d_{opt}$, there is $P_R = P_V$, and the T_M is positively correlated with $2\pi\kappa^2/(vd)$, hence T_M decreases with d. Actually, this part has redundancy in the case of $P_{SNR} = 1$ so that the acquisition time is equal under different turbulences. In addition, the smaller the spiral pitch, the more redundancy and the longer the time. Furthermore, as the turbulence increases, $g_{B,\sigma}(\omega)$ decreases, thus the d_{opt} decreases gradually. Meanwhile, the τ decreases as $g_{B,\sigma}(\omega)$ decreases under the same d, resulting in the corresponding acquisition time increases. Consequently, the optimization conclusion of the spiral pitch is verified.

Figure 5 presents the variation of the multi-scan acquisition time with the beam divergence angle under different turbulences, where $d = 40\mu rad$ and $U = 1.3mrad$. The theoretical optimum divergence angle is calculated from Eq. (33). Analogously, the numerical results are an excellent match with the corresponding MC results. For level $Turb.5$, we get $B = 45.7\sigma^2 < 48.5\sigma^2 = B_{\sigma}^{\min}$ so that the acquisition time increases monotonically with the divergence angle, and the optimum is obtained at ω_{limit}. When turbulence level is $Turb.4$, although $B > B_{\sigma}^{\min}$, there still $\omega_{opt} = \omega_{limit}$ due to $\omega_{limit} < \omega_{eq}$ with $B = 58.3\sigma^2 < B_{\sigma}\left(W\left(g_{58.3\sigma^2,\sigma}(0.7\sigma)\right)\right) = 64\sigma^2$.

Table 1 Simulation Parameters

	Parameters	Value	Unit / Remark
Laser Communication Terminal onboard Satellite	Transmitter loss s_t	0.92	–
	Band-limited platform vibration	100	*Hz*
	Std. of platform vibration σ	4	*μrad*
	Std. of initial LoS error κ	1	*mrad*
	Scanning speed v	0.4	*mrad/s*
	Reset time T_a	10	*Sec.*
	Transmitter power P_t	80	*mW*
Optical Ground Station	Receiver loss s_r	0.92	–
	Receiver aperture diameter D_r	20	*cm*
	Proportion of split beam s_s	0.1	–
	Photoelectric response efficiency R_r	0.77	–
	Std. of noise current σ_n	10	*nA*
	Receiver average SNR threshold $\bar{Q}$	10	*dB*
	Field detection probability P_V	0.95	–
	Link distance R	1200	*km*
Channel	Turbulence parameters $(\gamma, \alpha, \beta, \sigma_I^2)$	(0.90, 21.6, 19.8, 0.10)	Turb.1 very weak level
		(0.58, 8.43, 6.92, 0.28)	Turb.2 weak level
		(0.36, 4.03, 1.54, 1.06)	Turb.3 medium level
		(0.27, 4.58, 1.24, 1.20)	Turb.4 strong level
		(0.21, 6.07, 1.08, 1.24)	Turb.5 very strong level

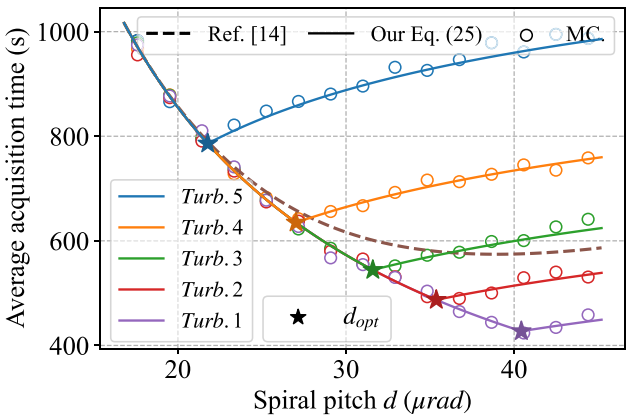

Fig. 4 The variation of the multi-scan acquisition time with the spiral pitch under different turbulences

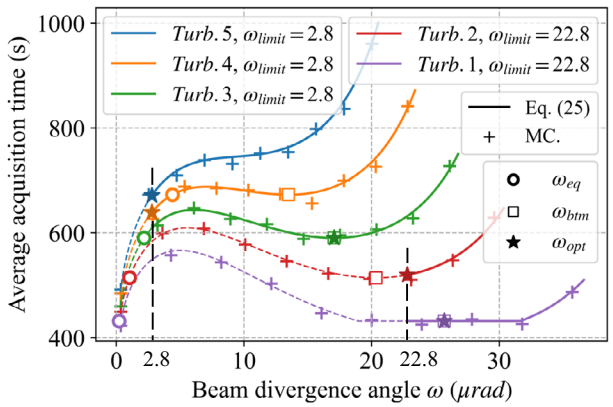

Fig. 5 The variation of the multi-scan acquisition time with the beam divergence angle under different turbulences. The dashed lines represent the part where $\omega < \omega_{limit}$

As the turbulence weakens, B increases and ω_{eq} decreases gradually. Then we obtain $\omega_{eq} < \omega_{limit}$ with $B = 75.1\sigma^2 > B_\sigma\left(W\left(g_{75.1\sigma^2,\sigma}(0.7\sigma)\right)\right) = 70\sigma^2$ at $Turb.3$, where the optimum divergence angle is taken at ω_{btm}. While $Turb.2$ with $B = 95.5\sigma^2 < B_\sigma(5.7\sigma) = 111.5\sigma^2$, $\omega_{btm} < \omega_{limit}$ is not within the feasible range thereby $\omega_{opt} = \omega_{limit}$. As the turbulence continues to weaken, B and ω_{btm} gradually increase. We get $\omega_{limit} < \omega_{btm}$ with $B = 137.3\sigma^2 > 111.5\sigma^2$ at $Turb.1$, where the optimum divergence angle is taken at ω_{btm}. Moreover, the acquisition time does not change with ω between $18.8\mu rad$ and $32\mu rad$, which is because $g_{B,\sigma}(\omega)/d > 1/2$ and single-scan acquisition probability remains constant. Consequently,

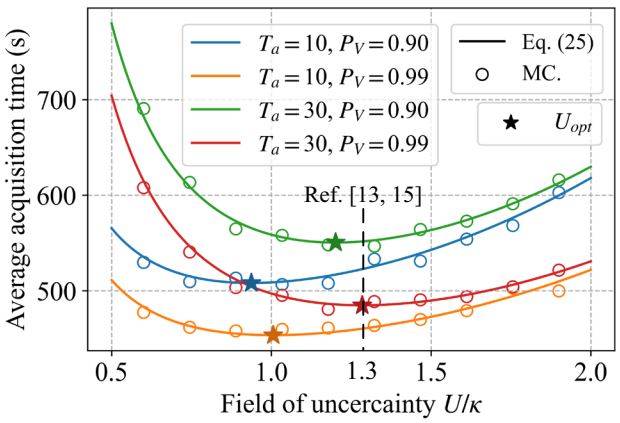

Fig. 6 The variation of the multi-scan acquisition time with the FOU under different combinations of reset time and field detection probability at turbulence level *Turb*.3

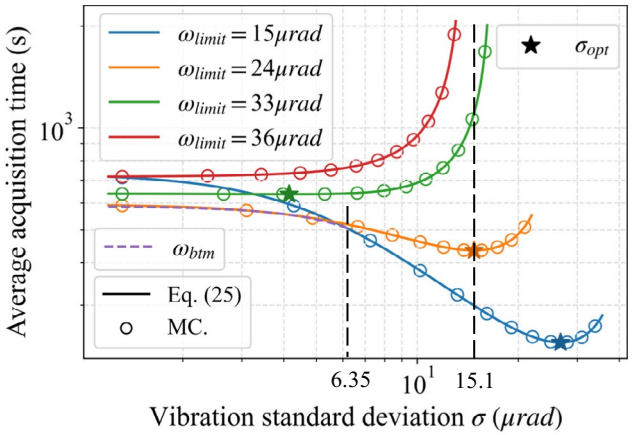

Fig. 7 The variation of the multi-scan acquisition time with the platform vibration level under different beam divergence angles at turbulence level *Turb*.3

the optimization conclusion of the beam divergence angle is verified.

Figure 6 shows the variation of the multi-scan acquisition time with the FOU under different combinations of reset time and field detection probability, where $\omega = 20\mu rad$, $d = 48\mu rad$, and turbulence level is *Turb*.3. The theoretical optimum FOU is fitted by Eq. (37). It can be observed that the change of reset time has a significant effect on the acquisition time when U is small. The acquisition time with $T_a = 30$ is larger than that with $T_a = 10$ by 38% at $U/\kappa = 0.5$. The influence gradually weakens as FOU increases until $U/\kappa = 2$ where the acquisition time with $T_a = 30$ is only 2% larger than that with $T_a = 10$. This is because the number of resets decreases as U increases, and the total reset time decreases. On the other hand, the T_U is proportional to the square of U, which is a higher-order term relative to T_a. Moreover, the increase of the field detection probability P_V means a larger single-scan acquisition probability, thus significantly reducing the acquisition time. Furthermore, the FOU was optimized with multi-scan as well in [13] and [15], obtaining the optimum FOU at $U/\kappa = 1.3$, but the difference from ground-truth U_{opt} is 1% in the case of $T_a = 30$ and $P_V = 0.99$, while the difference reaches 38.3% for $T_a = 10$ and $P_V = 0.9$. This is because that decreasing T_a or P_V, which were not considered in [13] and [15], reduces $\hat{T}_a$ and further lower U_{opt}. Additionally, the error of the fit U_{opt} from Eq. (37) and the corresponding T_M is within 0.2% and 10^{-4}%, respectively, which demonstrates that our optimization conclusion of FOU is more accurate.

Finally, Fig. 7 illustrates the variation of the multi-scan acquisition time with the platform vibration standard deviation under different beam divergence angles, where $d = 80\mu rad$, $U = 1.3mrad$, and turbulence level is *Turb*.3. When $\sigma < 6.3\mu rad$, there is $B > B_\sigma^{\min}$ so that ω_{btm} exists, the corresponding acquisition time T_M decreases with the increase of vibration level σ, which indicates that the vibration noise can be transformed into a favorable factor to improve the acquisition performance according to the optimization conclusion of divergence angle. For $\omega_{limit} = 36\mu rad > B^{1/2}e^{-1/4} = 34.3\mu rad$, the stronger the platform vibration, the longer the acquisition time. When σ is close to $14.1\mu rad$, the coverage factor is approximately zero, resulting in the acquisition time approaching infinity. For $\omega_{limit} = \{15, 24, 33\}\mu rad$, the minimum T_M exists at σ_{opt}, which increases with the decrease of ω_{limit}. This shows that reducing ω_{limit} can improve the acquisition performance in an increasing range of platform vibration levels. When $\sigma \geq 6.3\mu rad$, there is $B \leq B_\sigma^{\min}$ so that T_M increases with ω_{limit} at the same vibration level σ. Moreover, for $\omega_{limit} = 24\mu rad$, we obtain $\sigma_{opt} = 15.1\mu rad$, where the corresponding acquisition time is increased by 134 seconds and reduced by 640 seconds compared with that for $\omega_{limit} = 15\mu rad$ and $\omega_{limit} = 33\mu rad$, respectively. However, reducing ω_{limit} means a larger resonator and a more complex system. Although both reduce ω_{limit} by $9\mu rad$, the cost from $24\mu rad$ to $15\mu rad$ is geometrically increased compared with that from $33\mu rad$ to $24\mu rad$. In other words, the improvement of the acquisition performance by reducing the beam divergence angle after $\omega_{limit} = 24\mu rad$ is very limited at the same cost. This quantitatively demonstrates that designing ω_{limit} according to Eq. (39) achieves a good trade-off between the acquisition performance and complexity of the APT system.

5 Conclusion

In this paper, a multi-scan link acquisition time model based on the received average SNR is proposed for LEO-to-ground laser communication, where the parameters

of beam divergence angle, spiral pitch, and FOU are optimized to obtain the minimum acquisition time. Such derivations had not been presented yet. Compared with the existing models that assumed a successful acquisition when the receiver is within the divergence angle of the Gaussian beam, the proposed model takes the received average SNR as the criterion, which is suitable for various photoelectric sensors. Specifically, we present the concept of "coverage factor", denoting the maximum ratio of acquisition angle to spiral pitch wherein the receiver meets SNR level for a certain transmitted power. Under the combined effects of the platform vibration with Rice distribution and the Gamma-Gamma turbulence channel, we derive the required transmitted power as a function of beam divergence angle, spiral pitch, and coverage factor for SNR threshold. For LEO-to-ground FSOC with a limited narrow window, the scanning needs to maintain the maximum transmitted power to achieve fast acquisition, thereby these parameters are decoupled at a fixed power. Subsequently, the probability distribution of coverage factor is derived based on the initial pointing error obeying Rayleigh distribution, which allows us to calculate the probability that the received SNR exceeds the threshold. Combined with FOU and receiver field angle, we obtain the single-scan acquisition probability, which is less than one, so that the multi-scan is adopted to ensure acquisition success. Considering the essential reset time between single-scan, we establish a novel multi-scan acquisition time model and present optimizations. The numerical results calculated by the proposed analytical expressions are consistent with the MC simulations. Due to the combination of turbulence, the proposed model is also applicable to the inter-satellite FSOC scenario. Moreover, the quantitative analysis of the influence of platform vibration indicates that the vibration noise will be transformed into a favorable factor to improve the acquisition performance in an increasing range of vibration levels as the decrease of the minimum divergence angle modulated by the laser. Furthermore, we present a theoretical method for designing the minimum divergence angle, which achieves a good trade-off between the link acquisition performance and complexity of the APT system. Overall, this work provides important theoretical support for the design of beaconless LEO-to-ground FSOC system.

Author Contributions SY carried out the derivations, performed the simulations, and wrote the main manuscript. XL supervised the project. All authors reviewed the manuscript.

Funding The authors did not receive support from any organization for the submitted work.

Data availability Data sets generated during the current study are available from the corresponding author on reasonable request.

Declarations

Conflict of interest All authors certify that they have no affiliations with or involvement in any organization or entity with any financial interest or non-financial interest in the subject matter or materials discussed in this manuscript.

References

1. M. Toyoshima, W.R. Leeb, H. Kunimori, T. Takano, Comparison of microwave and light wave communication systems in space applications. Opt. Eng. **46**(1), 015003 (2007)
2. M. Toyoshima, Trends in satellite communications and the role of optical free-space communications. J. Opt. Netw. **4**(6), 300–311 (2005)
3. I.I. Kim, B. Riley, N.M. Wong, M. Mitchell, W. Brown, H. Hakakha, P. Adhikari, E.J. Korevaar, Lessons learned for strv-2 satellite-to-ground lasercom experiment. In: Free-Space Laser Communication Technologies XIII, vol. 4272, pp. 1–15 (2001). SPIE
4. R. Fields, D. Kozlowski, H. Yura, R. Wong, J. Wicker, C. Lunde, M. Gregory, B. Wandernoth, F. Heine, 5.625 gbps bidirectional laser communications measurements between the nfire satellite and an optical ground station. In: 2011 International Conference on Space Optical Systems and Applications (ICSOS), pp. 44–53 (2011). IEEE
5. M. Gregory, F. Heine, H. Kämpfner, R. Meyer, R. Fields, C. Lunde, Tesat laser communication terminal performance results on 5.6 gbit coherent inter satellite and satellite to ground links. In: International Conference on Space Optics-ICSO 2010, vol. 10565, pp. 324–329 (2017). SPIE
6. P.W. Young, L.M. Germann, R. Nelson, Pointing, acquisition, and tracking subsystem for space-based laser communications. In: Optical Technologies for Communication Satellite Applications, vol. 616, pp. 118–128 (1986). SPIE
7. G. Picchi, G. Prati, D. Santerini, Algorithms for spatial laser beacon acquisition. IEEE Trans. Aerospace Electron. Syst. **2**, 106–114 (1986)
8. S. Yu, F. Wu, Q. Wang, L. Tan, J. Ma, Theoretical analysis and experimental study of constraint boundary conditions for acquiring the beacon in satellite-ground laser communications. Opt. Commun. **402**, 585–592 (2017)
9. S. Hu, H. Yu, Z. Duan, Y. Zhu, C. Cao, M. Zhou, G. Li, H. Liu, Multi-parameter influenced acquisition model with an in-orbit jitter for inter-satellite laser communication of the lces system. Opt. Express **30**(19), 34362–34377 (2022)
10. T.-H. Ho, Pointing, acquisition, and tracking systems for free-space optical communication links. (2007)
11. C. Hindman, L. Robertson, Beaconless satellite laser acquisition-modeling and feasability. In: IEEE MILCOM 2004. Military Communications Conference, 2004., vol. 1, pp. 41–47 (2004). IEEE
12. U. Sterr, M. Gregory, F. Heine, Beaconless acquisition for isl and sgl, summary of 3 years operation in space and on ground. In: 2011 International Conference on Space Optical Systems and Applications (ICSOS), pp. 38–43 (2011). IEEE
13. X. Li, S. Yu, J. Ma, L. Tan, Analytical expression and optimization of spatial acquisition for intersatellite optical communications. Opt. Express **19**(3), 2381–2390 (2011)

14. L. Friederichs, U. Sterr, D. Dallmann, Vibration influence on hit probability during beaconless spatial acquisition. J. Lightwave Technol. **34**(10), 2500–2509 (2016)
15. J. Ma, G. Lu, L. Tan, S. Yu, Y. Fu, F. Li, Satellite platform vibration influence on acquisition system for intersatellite optical communications. Opt. Laser Technol. **138**, 106874 (2021)
16. Z. Qiu, L. Lin, L. Chen, An active method to improve the measurement accuracy of four-quadrant detector. Opt. Lasers Eng. **146**, 106718 (2021)
17. S. Yang, X. Li, Iterative framework for a high accuracy aberration estimation with one-shot wavefront sensing. Opt. Express **30**(21), 37874–37887 (2022)
18. M. Nouri, A. Ghadimi, Reduction of dark current and gain increase in inas avalanche photodiode with algaas blocking layer. Optik **148**, 268–274 (2017)
19. H. Kaushal, G. Kaddoum, Optical communication in space: Challenges and mitigation techniques. IEEE Commun. Surveys Tutorials **19**(1), 57–96 (2016)
20. G. Hechenblaikner, S. Delchambre, T. Ziegler, Optical link acquisition for the lisa mission with in-field pointing architecture. Opt. Laser Technol. **161**, 109213 (2023)
21. H. Hemmati, Near-earth laser communications, second edition. (2020)
22. Iskander: A low-profile archimedean spiral antenna using an ebg ground plane. IEEE antennas and wireless propagation letters **3**, 223–226 (2004)
23. J. Wang, Y. Song, H. Jiang, T. Wang, K. Dong, Y. Liu, High-precision dynamic pointing method for improving the acquisition performance of laser communication between high-altitude platform stations. Optik **275**, 170621 (2023)
24. L.C. Andrews, R.L. Phillips, *Laser beam propagation through random media* (Second Edition, Laser Beam Propagation Through Random Media, 2005)
25. F. Wang, D. Jiang, Z. Wang, J. Chen, T.Q. Quek, Dynamic networking for continuable transmission optimization in leo satellite networks. IEEE Transactions on Vehicular Technology (2022)
26. W.O. Popoola, E. Poves, H. Haas, Spatial pulse position modulation for optical communications. J. Lightwave Technol. **30**(18), 2948–2954 (2012)
27. Q. Li, M. Wen, B. Clerckx, S. Mumtaz, A. Al-Dulaimi, R.Q. Hu, Subcarrier index modulation for future wireless networks: Principles, applications, and challenges. IEEE Wirel. Commun. **27**(3), 118–125 (2020)
28. A. Jurado-Navas, J.M. Garrido-Balsells, J.F. Paris, M. Castillo-Vázquez, A. Puerta-Notario, Impact of pointing errors on the performance of generalized atmospheric optical channels. Opt. Express **20**(11), 12550–12562 (2012)
29. M. Toyoshima, T. Jono, K. Nakagawa, A. Yamamoto, Optimum divergence angle of a gaussian beam wave in the presence of random jitter in free-space laser communication systems. JOSA A **19**(3), 567–571 (2002)
30. S.O. Rice, Statistical properties of a sine wave plus random noise. Bell Syst. Tech. J. **27**(1), 109–157 (1948)
31. A. Al-Habash, L.C. Andrews, R.L. Phillips, Mathematical model for the irradiance probability density function of a laser beam propagating through turbulent media. Opt. Eng. **40**(8), 1554–1562 (2001)
32. N. Wang, J. Cheng, Moment-based estimation for the shape parameters of the gamma-gamma atmospheric turbulence model. Opt. Express **18**(12), 12824–12831 (2010)
33. A. Prokeš, Modeling of atmospheric turbulence effect on terrestrial fso link. Radioengineering **18**(1), 42–47 (2009)

Publisher's Note Springer Nature remains neutral with regard to jurisdictional claims in published maps and institutional affiliations.

Springer Nature or its licensor (e.g. a society or other partner) holds exclusive rights to this article under a publishing agreement with the author(s) or other rightsholder(s); author self-archiving of the accepted manuscript version of this article is solely governed by the terms of such publishing agreement and applicable law.